Catalysis Science & Technology

ROYAL SOCIETY OF CHEMISTRY

COMMUNICATION

View Article Online
View Journal | View Issue



Cite this: *Catal. Sci. Technol.*, 2022, 12, 6363

Received 13th September 2022,
Accepted 7th October 2022

DOI: 10.1039/d2cy01596j

rsc.li/catalysis



# Understanding the geometric and basicity effects of organic polymer modifiers on $Ru/TiO_2$ catalysts for $CO_2$ hydrogenation to hydrocarbons†

Chengshuang Zhou[a] and Matteo Cargnello *[ab]

**Modifying inorganic catalysts with basic organic moieties effectively enhances their $CO_2$ hydrogenation activity through $CO_2$ activation, but the effect on C–C coupling rates and selectivity is not as straightforward. In this contribution, we report the encapsulation of $Ru/TiO_2$ catalysts with uniform, conformal, nitrogen-containing polymer overlayers with controllable basicity and morphology. We demonstrate that while basic moieties greatly promote $CO_2$ conversion, it is the morphology of the overlayer that has a significant role in C–C coupling and the production of higher hydrocarbons.**

Activation of chemically inert $CO_2$ has long been considered the rate determining step for $CO_2$ utilization, including $CO_2$ hydrogenation to produce fuels and chemicals of interest.[1–4] Functionalizing catalysts with organic moieties,[5–10] especially those that possess Lewis basic character, such as organic amines, has thus proved to be a powerful tool to enhance $CO_2$ hydrogenation activity by electronic interactions of $CO_2$ with active sites and between organic ligands and reaction intermediates.[11–16] There has been overall less focus on the effect of organic moieties on C–C coupling and higher hydrocarbon production, mostly because most organic ligand modifiers are unstable at conditions that are relevant for C–C coupling, such as high temperature (220–320 °C) and pressure (10–30 bar).[7,13] Additionally, it is challenging to precisely control the spatial distribution of liner organic amines on catalyst surfaces, often leading to uncontrollable blocking of active sites, which will in turn affect the intrinsic activity of the resulting catalyst ensembles. Thus, systematic understanding that carefully decouples the geometric effect from basicity effects are crucial to obtain mechanistic understanding on the effect of organic modifications.

Our group previously reported a method to uniformly encapsulate $Ru/TiO_2$ catalysts with imine-based porous organic polymers (IPOP) and we discussed a morphology effect of polymers on C–C coupling and hydrocarbon production by $CO_2$ hydrogenation.[16] Thanks to their high degree of polymerization and aromatic content, the IPOPs are stable during $CO_2$ hydrogenation at 250 °C, 6 bar. The ensemble size of the active sites at the metal/polymer interface are not only predictable but also tuneable by varying the monomer precursor geometry (Fig. 1). Meanwhile, thanks to the versatile nature of the imine-condensation polymerization process, the polymer functionality can be engineered while maintaining similar geometry and pore sizes by including functional monomers. Here specifically, we extend the encapsulation approach to phthalaldehyde monomers with *meta*-connectivity but different chemical functionality to examine the effect of basicity on $CO_2$ hydrogenation.

A benchmark $Ru/TiO_2$ catalyst was prepared by impregnation of 5 nm Ru colloidal particles on $TiO_2$ supports and was used as a starting material for every other catalyst preparation. Using $Ru/TiO_2$ as substrate, imine-condensation reaction between 1,3,5-tris(4-aminophenyl)benzene and phthalaldehyde with different functional groups was carried out to produce a porous polymer overlayer growth on the support, forming three catalysts encapsulated by imine-polymers, namely *m*-IPOP/$Ru/TiO_2$, OH-IPOP/$Ru/TiO_2$ and py-IPOP/$Ru/TiO_2$, as shown in Fig. 1. py-IPOP/$Ru/TiO_2$ was further treated with $NaBH_4$ to reduce the imine group to a secondary amine, and py-APOP/$Ru/TiO_2$ was formed.[14] Fourier-transform infrared characterization demonstrates that $Ru/TiO_2$ showed broad –OH stretching features from 3000 to 3700 $cm^{-1}$, indicative of the hydroxyl groups present on the support surface (Fig. 2A). Instead, all polymer-encapsulated samples showed attenuated if not absent –OH stretching, indicating polymer growth on the $TiO_2$ surface

[a] *Department of Chemical Engineering, Stanford University, Stanford, CA 94305, USA. E-mail: mcargnello@stanford.edu*
[b] *SUNCAT Center for Interface Science and Catalysis, Stanford University, Stanford, CA 94305, USA*

† Electronic supplementary information (ESI) available. See DOI: https://doi.org/10.1039/d2cy01596j

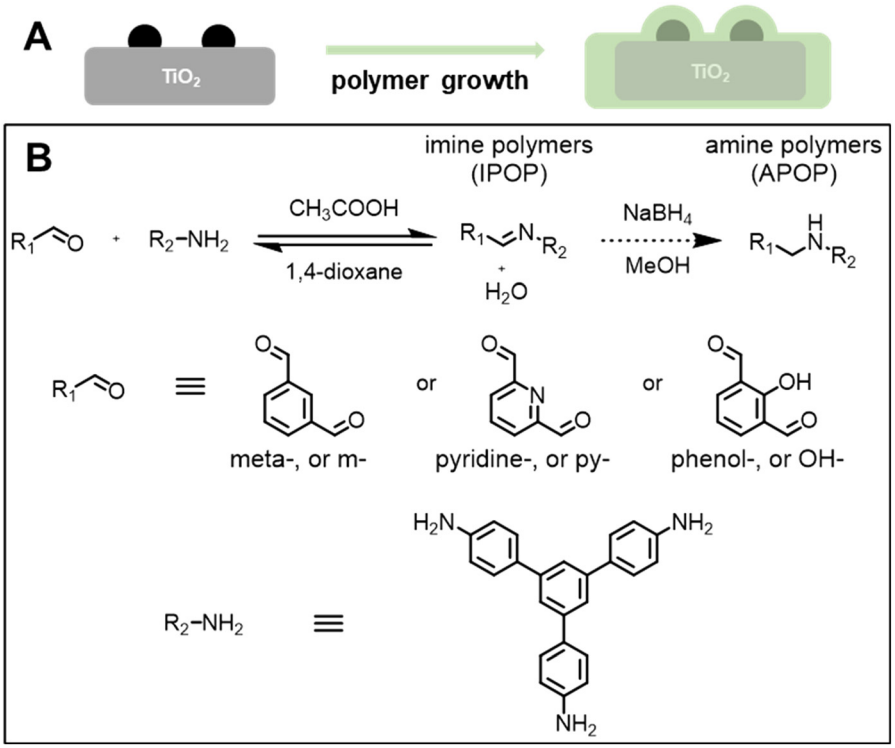


**Fig. 1** (A) Schematic of the synthesis process. Imine-based porous organic polymers (IPOP) with different functional groups were grown on Ru/$TiO_2$ catalyst used as a substrate. The IPOP/Ru/$TiO_2$ catalyst was further reduced to form amine-containing porous organic polymer (APOP) layers. (B) Simplified chemical reactions involved in the synthesis process.

(Fig. 1A). Characteristic C═N vibrations from the imine linkages could be discerned at ~1625 $cm^{-1}$ for *m*-IPOP, OH-IPOP and py-IPOP/Ru/$TiO_2$. py-APOP/Ru/$TiO_2$, on the other hand, showed rather intense N–H bending feature at 1610

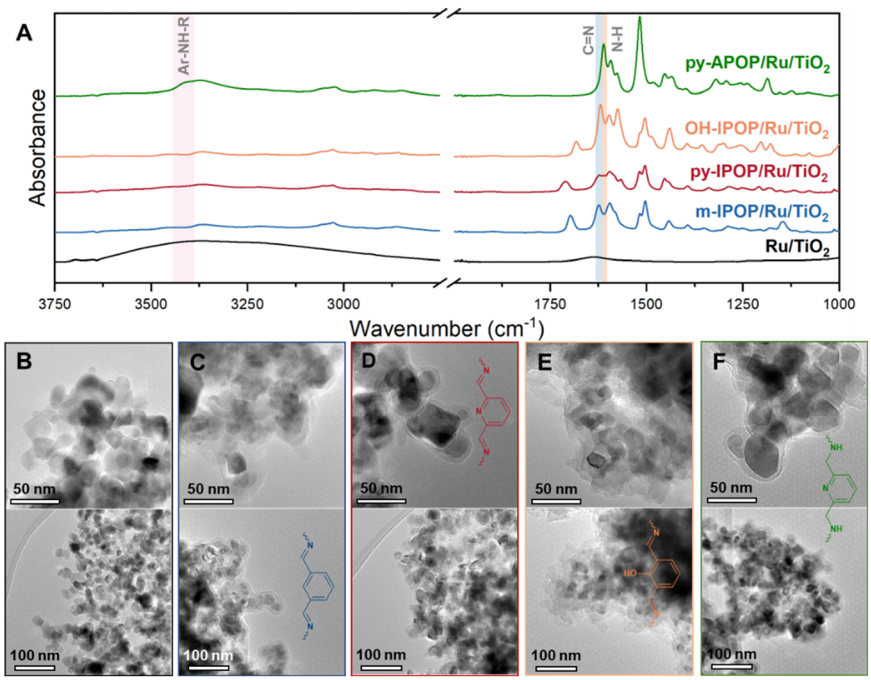


**Fig. 2** (A) Attenuated total reflectance infrared spectra and (B–F) representative transmission electron microscopy images of the catalysts prepared in this work: Ru/TiO2 (B), *m*-IPOP/Ru/$TiO_2$ (C), py-IPOP/Ru/$TiO_2$ (D), OH-IPOP/Ru/$TiO_2$ (E), and py-APOP/Ru/$TiO_2$ (F).

 

$cm^{-1}$ and N–H stretching feature around 3415 $cm^{-1}$, which indicate the successful conversion of C═N to C–N bond with consequent increase in basicity among all samples. TEM images of the hybrid samples reveal that the encapsulation of the $Ru/TiO_2$ was uniform and conformal, as the low-contrast polymer layer followed closely the contour of the underlying $TiO_2$ particles (Fig. 2C–F). The average polymer thickness was measured to be ~10 nm for all encapsulated samples, suggesting that the organic fraction in the samples is similar, which also agrees with thermogravimetric analysis (TGA) (see below).

X-ray photoelectron spectroscopy (XPS) spectra were collected to verify the encapsulation and the different chemical properties of the catalysts. Distinct and intense peaks related to Ti species can be distinguished in $Ru/TiO_2$ sample, which is expected (Fig. 3A and D). While peaks higher than 462 eV originate from spin–orbit splitting, the presence of both peaks at 459.9 eV and 458.0 eV indicate that the $TiO_2$ surface is slightly reduced, likely due to oxygen vacancy formation from high temperature calcination and water removal. The peaks in the O 1s region agree with such analysis, including saturated lattice oxygen at 530.9 eV, oxygen near vacancies at 529.1 eV and one additional peak at 532.7 eV from adventitious organic contaminants. On the other hand, Ti and O signal were greatly attenuated and difficult to identify for all encapsulated catalysts, proving that the polymer layers are at least ~5–10 nm thick so that the photoemitted electrons from the underneath $TiO_2$ layer can hardly escape. The peak at ~533.0 eV is attributed to hydroxyl groups in OH-IPOP/$Ru/TiO_2$, which appeared to be weak when plotted on the same scale as $Ru/TiO_2$.

The Ti 2p and O 1s regions provided no information for the encapsulated samples, however, the C 1s and N 1s regions were crucial in understanding the differences between the polymer overlayers (Fig. 3B and C). All encapsulated catalysts showed signals indicative of the carbon framework (284.8 eV, noted as C–C) and the carbons bonded to nitrogen species (286.5 eV, noted as C–N). The intrinsic elemental N/C ratio from different polymer overlayers were well reflected by the relative C–N/C–C peak area, with a N/C ratio of 0.5 for py-IPOP and py-APOP and a ratio of 0.3 for *m*-IPOP and OH-IPOP bearing less nitrogen. Additional features above 290.0 eV were attributed to the π–π conjugation of stacked aromatic rings, again confirming the conformal nature of polymer overlayers at the polymer/oxide interfaces. Finally, when examining N 1s peaks, we could clearly identify that *m*-IPOP and OH-IPOP shared peaks at similar position at ~399.1 eV, while py-IPOP showed a slightly shifted peak at 399.5 eV and py-APOP showed an even further shifted peak at 399.8 eV. It is difficult to discern the individual components through fitting since all nitrogen atoms are directly bonded to aromatic rings and the binding energies are similar for highly conjugated nitrogen species.[17] However, the observation is in very good agreement with

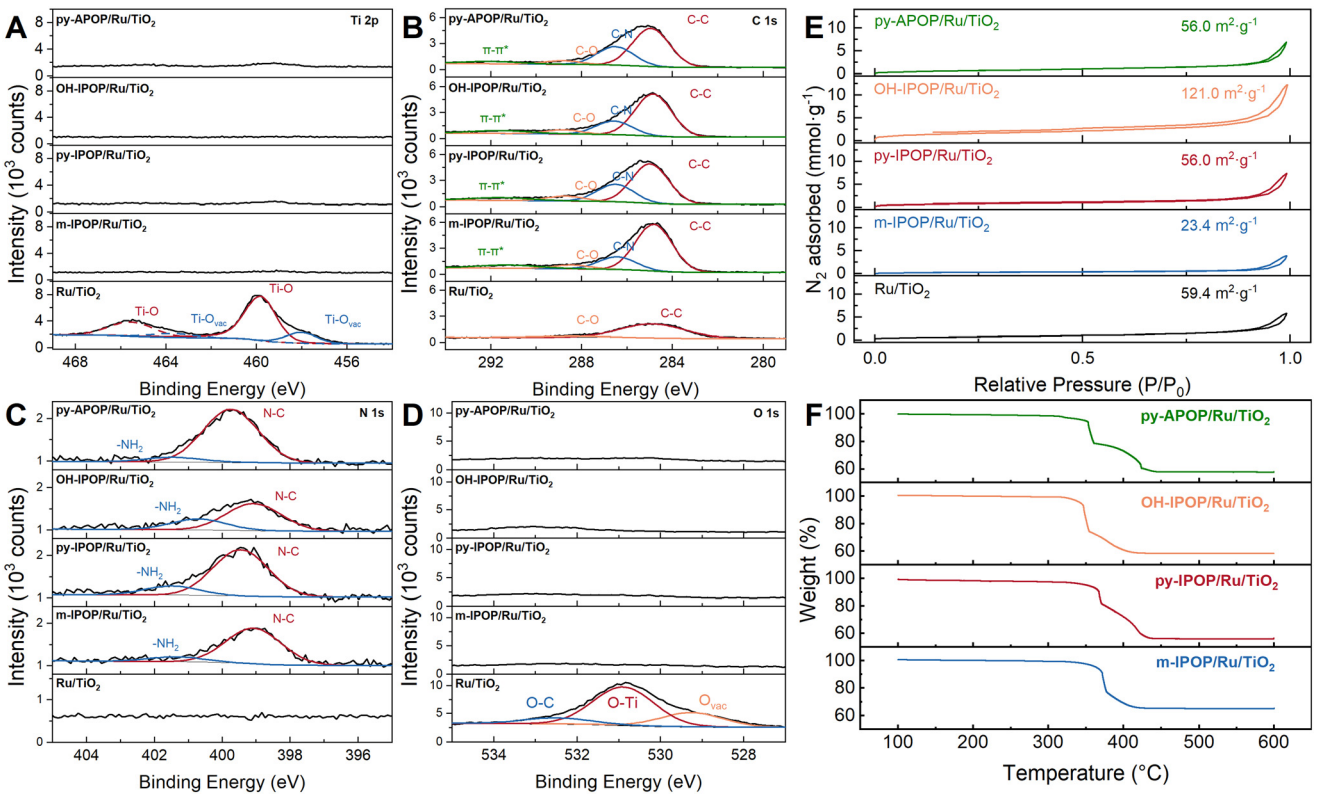


**Fig. 3** (A) Ti 2p, (B) C 1s, (C) N 1s and (D) O 1s X-ray photoelectron spectroscopy spectra, (E) $N_2$ physisorption isotherms and (F) thermogravimetric analysis of the catalysts. Black traces in (A–D) represent original data while coloured traces represent fitted components.

previous reports where imines and amines were qualitatively compared, and a shift of N 1s peak towards higher binding energy indicate a transition from N=C imine bond to NH-CH amine bond.[14]

All encapsulated samples have similar nitrogen adsorption isotherm profiles compared to the $Ru/TiO_2$ substrate (Fig. 3E). The IPOP overlayers are analogous to covalent organic frameworks (COFs), which usually show high surface areas and micro- or meso-porous-type isotherms, so higher specific surface areas were expected from the coating.[18–20] We postulate that the overlayers present in our study are thin and conformal such they do not notably alter the surface morphology of $TiO_2$ particles, resulting in similar isotherms and specific surface area values due to the fact that increased surface area and added mass from IPOP balance each other out. We wish to highlight that, based on the similar surface area and surface texture, the polymer overlayers are unlikely to notably affect the diffusion of gaseous reactants and products in a way that is responsible for the differences in catalytic activity.

Finally, we performed thermogravimetric analysis to test the thermal stability of encapsulated samples. The results revealed that IPOP moieties remained stable until at least 340 °C, and the mass-loss up to 250 °C was less than 2% (Fig. 3F). These results demonstrate that these catalysts are excellent candidates for stable $CO_2$ hydrogenation reaction at 250 °C. By fully combusting the polymeric components at 600 °C, we were able to quantify the organic mass fraction of the encapsulated samples, which were 35%, 44%, 42%, 42% for *m*-IPOP, py-IPOP, OH-IPOP and py-APOP/$Ru/TiO_2$, respectively. The similarity in organic mass fractions corroborated the similarity in layer thickness observed in Fig. 2 by TEM.

The catalysts were then tested for $CO_2$ hydrogenation in a mixture of 75% $H_2$ and 25% $CO_2$ at 250 °C up to 10 bar of pressure, conditions at which the IPOPs were completely stable, both verified in our previous report[16] and in this work (Fig. S5 and S6†). Specifically, we found that the FT-IR and XPS spectra of the catalysts after catalysis tests remained almost identical to those of as-synthesized catalysts, except for signals affected by the diluent used in the catalytic reaction (SiC). The amount of catalyst (based on the mass of Ru) across tests was adjusted to be similar so that the $CO_2$ conversion can fairly represent the normalized activity of different catalysts, summarized in Fig. 4. We observed that the benchmark catalyst, $Ru/TiO_2$, was highly active for $CO_2$

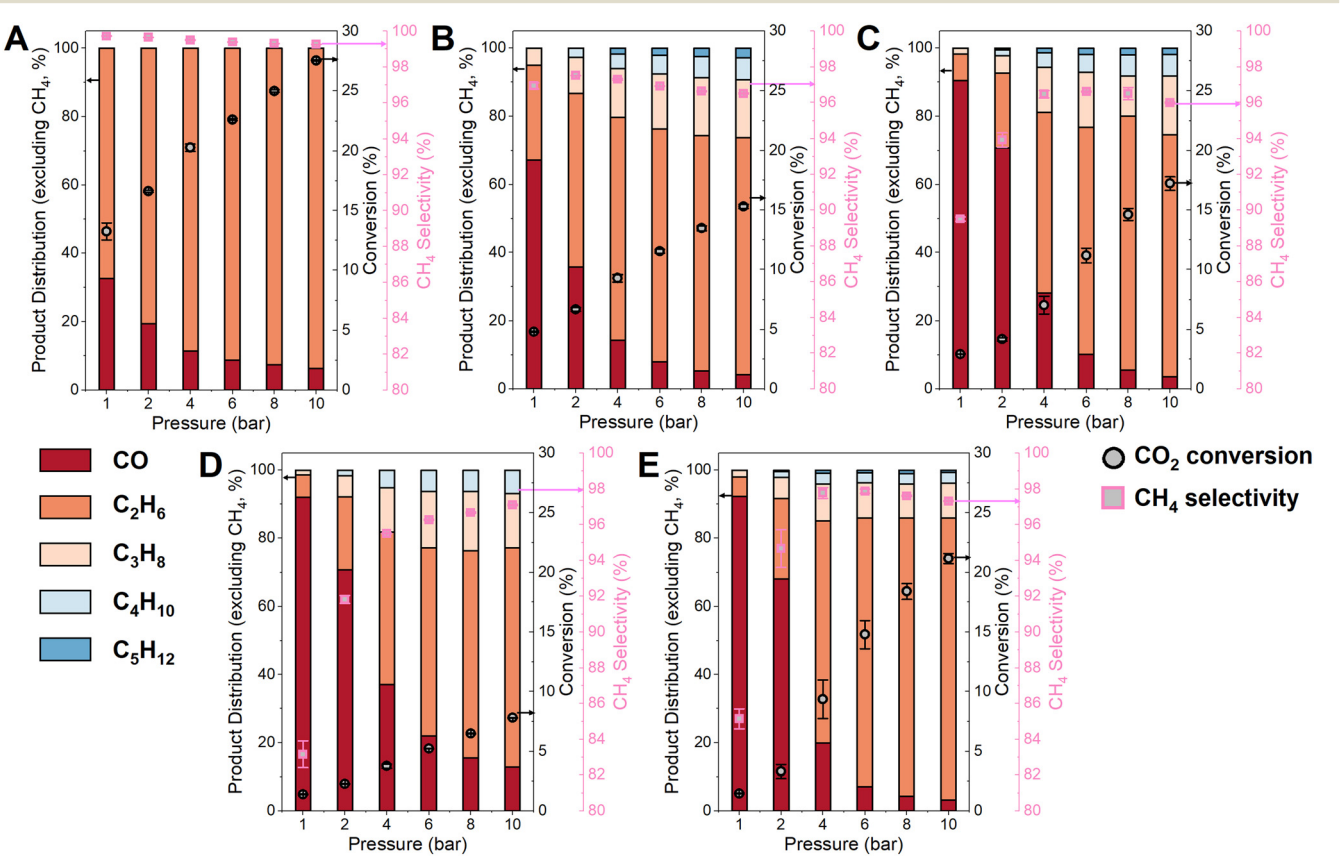


**Fig. 4** Catalytic performance of (A) $Ru/TiO_2$, (B) *m*-IPOP/$Ru/TiO_2$, (C) py-IPOP/$Ru/TiO_2$, (D) OH-IPOP/$Ru/TiO_2$ and (E) py-APOP/$Ru/TiO_2$ for $CO_2$ hydrogenation. Reactions were performed at 250 °C under a flow of 30 mL $min^{-1}$ of 75% $H_2$ + 25% $CO_2$ and similar Ru mass loading, while varying total pressure.

 

methanation, starting with 13% $CO_2$ conversion at 1 bar and readily increasing to 27% at 10 bar. Although $CH_4$ selectivity slightly decreased with increasing pressure as longer hydrocarbons became favored at higher pressure, it remained greater than 99% for all conditions tested. The high methanation activity and low $C_{2+}$ selectivity are consistent with other reports in the field,[21–23] being a combined result of high hydrogen and formate intermediates coverage and low coverage of adsorbed CO, as we highlighted in our previous work. Encapsulation by different IPOPs introduced two major effects affecting the pressure dependence and the $C_{2+}$ hydrocarbon selectivity of the catalysts (Fig. 4B–E). On one side, $CH_4$ selectivity was 97%, 89%, 83% and 85% for *m*-IPOP, py-IPOP, OH-IPOP and py-APOP/Ru/$TiO_2$ catalysts at ambient pressure, respectively, which were lower than that of Ru/$TiO_2$. The selectivity to methane increased to similar levels as total pressure was increased to 10 bar. On the other side, encapsulation greatly promoted the production of longer hydrocarbons, and linear hydrocarbons up to pentane ($C_5$) were detected from *m*-IPOP, py-IPOP and py-APOP/Ru/$TiO_2$, while butane ($C_4$) was detected from OH-IPOP/Ru/$TiO_2$. These results are all in qualitative agreement with our previous finding, and close examination will reveal the effect of polymer chemistry by comparing the differences in the catalytic performances.

We identify $CO_2$ conversion rate and $C_{3+}$ yield rate as important parameters that represent the potential of catalysts for $CO_2$ hydrogenation into value-added products. It is worth pointing out that we are comparing rates normalized by both Ru mass and exposed Ru surface, since the former is related to the catalyst cost efficiency, while the latter (turnover-frequency, TOF, normalized by chemisorption results shown in Table S1†) is related to the intrinsic reaction kinetics. Although IPOP encapsulation slightly reduced the $CO_2$ conversion rate per catalyst mass, likely due to blockage of some Ru sites, the TOF was significantly increased as the basicity of organic moieties increased (Fig. 5A). Specifically, the $CO_2$ hydrogenation TOF increased two-fold, four-fold and six-fold when Ru/$TiO_2$ was encapsulated by *m*-IPOP, py-IPOP and py-APOP, respectively, which show increasing basicity. In line with this result, encapsulation by more acidic OH-IPOP slightly decreased the $CO_2$ hydrogenation TOF.

The correlation between $CO_2$ hydrogenation activity and overlayer basicity corroborated our hypothesis that basic organic moieties interact more strongly with $CO_2$ and more effectively lower the entropic barrier of $CO_2$ activation, which is considered the rate determining step in $CO_2$ hydrogenation. The relationship between basicity and $C_{3+}$ production activity follows a slightly different trend, however, as both the mass-based rates and site-based TOFs first increased with basicity from OH-IPOP and *m*-IPOP to py-IPOP, to then decrease as the basicity was further increased in py-APOP. The initial increase agrees with previous analysis of total $CO_2$ conversion rate in that overlayers with increasing basicity facilitate the activation and conversion of $CO_2$. The latter decrease was however unexpected, and the C–C coupling probability was examined to gain a stronger mechanistic understanding (Fig. 5C). Interestingly, although $CO_2$ conversion activity was strongly correlated with polymer basicity, C–C coupling probability was only affected by the presence of the polymer but was not a function of polymer basicity. For example, C–C coupling was greatly promoted

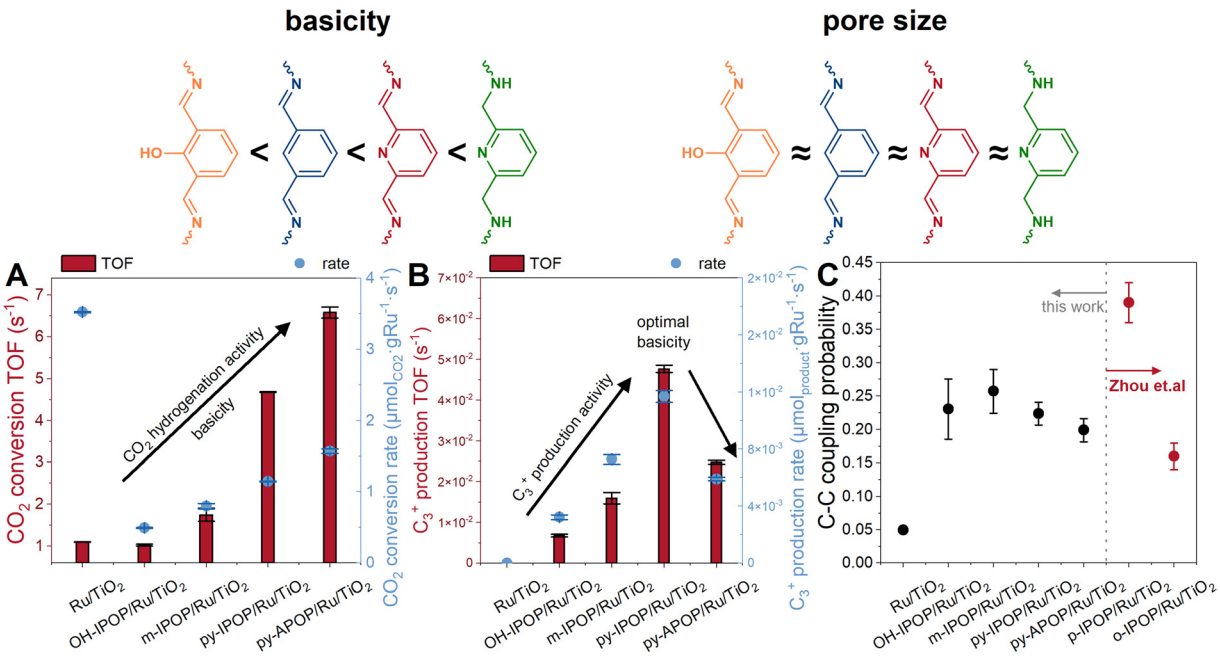


**Fig. 5** Comparison of (A) normalized $CO_2$ conversion rate (TOF), (B) $C_3^+$ hydrocarbon production rate and (C) C–C coupling probability of different catalysts at 250 °C, 30 mL $min^{-1}$ of 75% $H_2$ + 25% $CO_2$, 10 bar total pressure. Data in (C) refers to ref. 16.

when $Ru/TiO_2$ was encapsulated by OH-IPOP as the probability rose from 0.05 to 0.23, even slightly increased to 0.26 with *m*-IPOP, but then decreased to 0.22 and 0.20 with more basic py-IPOP and py-APOP encapsulation (Fig. 5C). Since C–C coupling is not notably affected by polymer basicity, we surmise that the size of the polymeric aperture, determined by the conformation of monomers, is the most decisive factor affecting C–C coupling. This element explains the similarities between all encapsulated catalysts studied here, given that they were synthesized using *meta*-substituted dialdehydes.

Our hypothesis is further supported when comparing the coupling probability in this study to those of similarly encapsulated catalysts with *para*- and *ortho*-substituted dialdehydes from our previous work.[16] We postulate that, given the conformal nature of the IPOP overlayers, the morphology of the polymer has a direct impact on the ensemble sizes at the metal/polymer interfaces. An appropriate ensemble on the Ru surface that is large enough to accommodate C–C coupling, but not too large so that undesired spectator species such as formate are formed, is desired to facilitate $C_{2+}$ production with higher selectivity. The C–C coupling probability will be notably enhanced when active site ensembles on $Ru/TiO_2$ catalyst surface were modified by the presence of any polymers with *meta*-substituted dialdehydes such as OH-IPOP, *m*-IPOP and py-IPOP. Further increasing the basicity to py-APOP likely also introduced more flexibility to the polymer framework through the free rotation about the C–N single bond and thus negatively impacted the polymer conformality at the metal/polymer interface.

## Conclusions

In this work, we have synthesized a series of polymer-encapsulated $Ru/TiO_2$ catalysts and examined the effect of the organic overlayer functional groups on the metal/polymer interface for $CO_2$ hydrogenation. We found that the $CO_2$ hydrogenation rate was notably enhanced by introduction of basic organic moieties surrounding Ru, likely through the facilitation of $CO_2$ activation by acid–base interactions. The C–C coupling probability did not show clear correlation with the polymer functionality and was instead more notably affected by the polymer conformation. As a combined result of $CO_2$ hydrogenation rate and C–C coupling probability, encapsulation by the polymer with higher basicity and appropriate pore size, namely py-IPOP, improved the $CO_2$ hydrogenation TOF of $Ru/TiO_2$ six-fold and greatly promoted $C_{3+}$ production, which was never detected in the comparison $Ru/TiO_2$ catalyst. Combined with our previous work, our findings here suggest that approaches to improve long-chain hydrocarbon production from $CO_2$ hydrogenation should carefully balance the promotion of $CO_2$ hydrogenation activity and the C–C coupling probability, as excessively increasing the $CO_2$ rate may also undesirably promote hydrogen activation towards undesired methane formation. Since the functional group and conformation of the polymer overlayer can be separately designed, encapsulation by porous polymers offers a promising approach to tune catalyst basicity and ensemble size independently and overcome scaling relationships. As a result, this strategy can lead to the development of a class of $CO_2$ hydrogenation catalysts with high activity and selectivity towards hydrocarbon production.

## Author contributions

C. Z. conducted all experiments and data analysis processes. C. Z. wrote the manuscript with input from M. C.

## Conflicts of interest

The authors declare no conflicts of interest.

## Acknowledgements

This work was supported by the Packard Foundation. Additional support was provided by a seed grant from the Precourt Institute of Energy at Stanford University. M. C. acknowledges support from a Sloan Fellowship, as well as the Novo Nordisk Center for $CO_2$ Research. Part of this work was performed at the Stanford Nano Shared Facilities, supported by the NSF under award ECCS-1542152.

## Notes and references

1 H. S. Shafaat and J. Y. Yang, *Nat. Catal.*, 2021, **4**, 928–933.
2 A. Wagner, C. D. Sahm and E. Reisner, *Nat. Catal.*, 2020, 1–12.
3 D. Goud, R. Gupta, R. Maligal-Ganesh and S. C. Peter, *ACS Catal.*, 2020, **10**, 14258–14282.
4 P. Gao, L. Zhang, S. Li, Z. Zhou and Y. Sun, *ACS Cent. Sci.*, 2020, **6**, 1657–1670.
5 L. O. Mark, C. Zhu, J. W. Medlin and H. Heinz, *ACS Catal.*, 2020, **10**, 5462–5474.
6 L. F. de L. e Freitas, B. Puértolas, J. Zhang, B. Wang, A. S. Hoffman, S. R. Bare, J. Pérez-Ramírez, J. W. Medlin and E. Nikolla, *ACS Catal.*, 2020, **10**, 5202–5207.
7 J. Zhang, L. D. Ellis, B. Wang, M. J. Dzara, C. Sievers, S. Pylypenko, E. Nikolla and J. W. Medlin, *Nat. Catal.*, 2018, **1**, 148–155.
8 G. Zakem, I. Ro, J. Finzel and P. Christopher, *J. Catal.*, 2021, **404**, 883–896.
9 V. Smeets, W. Baaziz, O. Ersen, E. M. Gaigneaux, C. Boissière, C. Sanchez and D. P. Debecker, *Chem. Sci.*, 2020, **11**, 954–961.
10 V. Smeets, L. Ben Mustapha, J. Schnee, E. M. Gaigneaux and D. P. Debecker, *Mol. Catal.*, 2018, **452**, 123–128.
11 A. Bordet, S. El Sayed, M. Sanger, K. J. Boniface, D. Kalsi, K. L. Luska, P. G. Jessop and W. Leitner, *Nat. Chem.*, 2021, **13**, 916–922.
12 G. Lee, Y. C. Li, J.-Y. Kim, T. Peng, D.-H. Nam, A. Sedighian Rasouli, F. Li, M. Luo, A. H. Ip, Y.-C. Joo and E. H. Sargent, *Nat. Energy*, 2021, **6**, 46–53.

 

13 J. Zhang, S. Deo, M. J. Janik and J. W. Medlin, *J. Am. Chem. Soc.*, 2020, **142**, 5184–5193.
14 H. Liu, J. Chu, Z. Yin, X. Cai, L. Zhuang and H. Deng, *Chem*, 2018, **4**, 1696–1709.
15 J. Kothandaraman, A. Goeppert, M. Czaun, G. A. Olah and G. K. S. Prakash, *J. Am. Chem. Soc.*, 2016, **138**, 778–781.
16 C. Zhou, A. S. Asundi, E. D. Goodman, J. Hong, B. Werghi, A. S. Hoffman, S. S. Nathan, S. F. Bent, S. R. Bare and M. Cargnello, *Proc. Natl. Acad. Sci. U. S. A.*, 2022, **119**, e2114768119.
17 M. Kehrer, J. Duchoslav, A. Hinterreiter, M. Cobet, A. Mehic, T. Stehrer and D. Stifter, *Plasma Processes Polym.*, 2019, **16**, 1800160.
18 W. Zhang, L. Chen, S. Dai, C. Zhao, C. Ma, L. Wei, M. Zhu, S. Y. Chong, H. Yang, L. Liu, Y. Bai, M. Yu, Y. Xu, X.-W. Zhu, Q. Zhu, S. An, R. S. Sprick, M. A. Little, X. Wu, S. Jiang, Y. Wu, Y.-B. Zhang, H. Tian, W.-H. Zhu and A. I. Cooper, *Nature*, 2022, **604**, 72–79.
19 L. Grunenberg, G. Savasci, M. W. Terban, V. Duppel, I. Moudrakovski, M. Etter, R. E. Dinnebier, C. Ochsenfeld and B. V. Lotsch, *J. Am. Chem. Soc.*, 2021, **143**, 3430–3438.
20 K. Geng, T. He, R. Liu, S. Dalapati, K. T. Tan, Z. Li, S. Tao, Y. Gong, Q. Jiang and D. Jiang, *Chem. Rev.*, 2020, **120**, 8814–8933.
21 H. Xin, L. Lin, R. Li, D. Li, T. Song, R. Mu, Q. Fu and X. Bao, *J. Am. Chem. Soc.*, 2022, **144**, 4874–4882.
22 A. Kim, C. Sanchez, G. Patriarche, O. Ersen, S. Moldovan, A. Wisnet, C. Sassoye and D. P. Debecker, *Catal. Sci. Technol.*, 2016, **6**, 8117–8128.
23 A. Aitbekova, L. Wu, C. J. Wrasman, A. Boubnov, A. S. Hoffman, E. D. Goodman, S. R. Bare and M. Cargnello, *J. Am. Chem. Soc.*, 2018, **140**, 13736–13745.